Scientia Iranica B (2013) 20 (1), 162–171

Sharif University of Technology

**Scientia Iranica**

*Transactions B: Mechanical Engineering*

www.sciencedirect.com

# Two-fluid analysis of a gas mixing problem

**I. Zahmatkesh** [a,*], **H. Emdad** [b], **M.M. Alishahi** [b]

[a] *Department of Mechanical Engineering, Mashhad Branch, Islamic Azad University, Mashhad, Iran*

[b] *School of Mechanical Engineering, Shiraz University, Shiraz, Iran*

Received 24 January 2012; revised 24 August 2012; accepted 29 October 2012

**KEYWORDS**

Two-fluid model;
Gas mixture;
Mixing;
Molecular interaction model;
Numerical simulation.

**Abstract** The mixing pattern of two parallel gas streams initially separated by a splitter plate is analyzed in this study. A recently proposed, two-fluid model is utilized for simulation of the flow field. The model provides separate balance equations for each component species of the system. As a consequence of the strong resemblance of the two-fluid model to the Navier–Stokes equations, the same numerical methods are applied to these new equations. The computations are undertaken for two-fluid systems; one with particles of about equal masses and another with particles of quite distinct masses, and the corresponding results are compared. This clarifies how the mass disparity of the constituents may affect the establishment of the flow field. The influence of molecular interaction descriptions in the model predictions is also examined by comparing the results of a hard-sphere model, the Maxwell repulsive potential, and the Lennard-Jones 12-6 potential.



## 1. Introduction

Gas mixture flows appear in diverse applications. Examples include pollutant dispersion, chemical processing, and combustor mixing and reaction. In these flows, several new phenomena can lead to somehow surprising behavior, compared with a single-component case. As an example, diffusion can be observed due to imposed pressure, temperature, and concentration gradients. Additionally, concentration gradients may lead to the transfer of heat.

When analyzing gas mixture flows, mixing is a critical issue; it controls the degree of pollutant dispersion. The rate of chemical reaction in many practical systems is also limited by the rate of mixing between the reactants. For these reasons, attention needs to be paid to the simulation of mixing processes.

Numerical models to predict gas mixture flows can be classified into two categories. In the first category, the fluid dynamics of a mixture (e.g., a binary system) is described by the Navier–Stokes equations for the mixture as a whole. An additional equation is also solved describing the conservation of mass for the first component species. This equation, in conjunction with the continuity equation for the whole mixture, implies the conservation of mass for the second component as well [1].

Models in the second category are, however, based on the gas kinetic theory. While several kinetic descriptions have been proposed (e.g. [2–6]), nearly all of them carry several simplifying assumptions in their constitutive relations, as well as their description of collision frequencies. This prohibits their use in practical problems with complex geometries. Consequently, application of these models has been restricted to simple mixture problems like Couette flow or one-dimensional shock propagation.

Based on the two-fluid theory and with a procedure similar to Goldman and Sirovich [2], but with some improvements in constitutive relations and collision terms, Kamali et al. [7] have recently derived a new set of balance equations for the flow of binary gas mixtures. The proposed model consists of a separate equation set for one component species of the system and an equation set for average quantities of the mixture. Thereby, it can automatically describe diffusion processes excluding the use of any coefficients for ordinary, pressure, and thermal diffusion, which are generally required during the Navier–Stokes computation of gas mixture problems. The

* Corresponding author. Tel.: +98 915 510 93 99.
*E-mail address:* zahmatkesh5310@mshdiau.ac.ir (I. Zahmatkesh).

Peer review under responsibility of Sharif University of Technology.

Production and hosting by Elsevier

1026-3098 © 2013 Sharif University of Technology. Production and hosting by Elsevier B.V. Open access under CC BY-NC-ND license.
doi:10.1016/j.scient.2012.12.017

**Nomenclature**

| | |
|---|---|
| $d$ | molecular diameter |
| $E$ | total energy per unit volume |
| $\tilde{E}$ | collision parameter |
| $\mathbf{F}$ | external force vector |
| $H$ | distance between the plates |
| $J$ | Jacobian of transformation |
| $k$ | Boltzmann constant |
| $\mathrm{Kn}_{\mathrm{overall}}$ | overall Knudsen number of the gas mixture |
| $L$ | characteristic length of the problem |
| $m$ | molecular mass |
| $m_{\alpha\beta}$ | reduced mass of the gas mixture |
| $M$ | molar mass |
| $M_{\alpha\alpha}$ | transport coefficient associated with thermal-diffusion effects |
| $M_{\beta\alpha}$ | transport coefficient associated with thermal-diffusion effects |
| $n$ | number density |
| $p$ | pressure |
| $p_e$ | exit pressure |
| $p_{t,i}$ | inlet stagnation pressure |
| $\mathbf{P}$ | partial pressure tensor |
| $\mathbf{q}$ | heat flux vector |
| $R$ | gas constant |
| $r$ | intermolecular separation |
| $t$ | time |
| $T$ | temperature |
| $T_{t,i}$ | inlet stagnation temperature |
| $\tilde{T}$ | collision parameter |
| $u, v$ | components of velocity vector |
| $\mathbf{v}$ | velocity vector |
| $\tilde{\mathbf{v}}$ | collision parameter |
| $W_{\alpha\beta}^{(i,j)}$ | non-dimensional Chapman–Cowling collision integrals |
| $x, y$ | Cartesian coordinates |

*Greek symbols*

| | |
|---|---|
| $\Gamma$ | Gamma function |
| $\gamma$ | ratio of the specific heats |
| $\delta_{ij}$ | Kronecker delta |
| $\varepsilon_{\alpha\beta}$ | maximum energy of attraction |
| $\eta$ | normal direction in the generalized curvilinear coordinates |
| $\eta_{\alpha\alpha}$ | transport coefficient associated with viscous effects |
| $\eta_{\alpha\beta}$ | transport coefficient associated with viscous effects |
| $\eta_{\beta\alpha}$ | transport coefficient associated with viscous effects |
| $\eta_{\beta\beta}$ | transport coefficient associated with viscous effects |
| $\kappa_{\alpha\beta}$ | constant coefficient in the force law |
| $\lambda_{\mathrm{overall}}$ | overall mean-free-path of the gas mixture |
| $\lambda_\alpha$ | mean-free-path of constituent $\alpha$ in the mixture |
| $\lambda_\beta$ | mean-free-path of constituent $\beta$ in the mixture |
| $\lambda_{\alpha\alpha}$ | transport coefficient associated with thermal effects |
| $\lambda_{\alpha\beta}$ | transport coefficient associated with thermal effects |
| $\lambda_{\beta\alpha}$ | transport coefficient associated with thermal effects |
| $\lambda_{\beta\beta}$ | transport coefficient associated with thermal effects |
| $\xi$ | streamwise direction in the generalized curvilinear coordinates |
| $\rho$ | mass density |
| $\sigma_{\alpha\beta}$ | distance at which the potential function of interaction vanishes |
| $\tau_{ij}$ | viscous stress tensor |
| $\upsilon_{\alpha\beta}$ | collision frequency for cross-collision between species $\alpha$ and $\beta$ molecules |
| $\upsilon_{\beta\alpha}$ | collision frequency for cross-collision between species $\beta$ and $\alpha$ molecules |
| $\phi_{\alpha\beta}$ | interparticle potential function |
| $\mathbf{\Omega}_{\alpha\beta}^{(i,j)}$ | Chapman–Cowling collision integrals |

*Subscripts*

| | |
|---|---|
| $\alpha, \beta$ | mixture constituents |

model also computes transport coefficients from some kinetic relations without the requirement of being input externally. This removes uncertainties associated with (i) transport coefficients of the constituents that are input and (ii) transport coefficients of the mixture as a whole that must be estimated in terms of properties of the constituents from some semi-empirical correlations. Since the derivation of the two-fluid model has been made without any limiting assumption or approximation, the resulting equations are applicable to arbitrary flow conditions. Consequently, it can be regarded as an effective simulation method for the study of gas mixture flows in engineering applications.

An alternative form of this two-fluid model has also been developed by Kamali et al. [8]. In contrast to the aforesaid description, this alternative formulation provides separate equation sets for each component species of the system. Consequently, the computational procedure utilized for the original form of the model needs some modifications before it becomes suitable for this formulation. This has been accomplished during a recent analysis of Zahmatkesh et al. [9] who presented viscous, as well as inviscid, solutions for some gas mixture problems in the context of a converging-diverging nozzle.

To continue these efforts, both forms of the developed two-fluid model that were applied with hard-sphere molecules have been extended to more realistic molecular interaction descriptions (i.e., Maxwell repulsive potential and Lennard-Jones 12-6 potential) [10]. Moreover, the contribution of external forces has been incorporated in the model equations [10].

In a subsequent attempt, the original form of the proposed two-fluid model has been employed for the simulation of parallel mixing of two gas streams, initially separated by a splitter plate [11]. The effect of temperature level on the degree of gas mixing was also clarified during that investigation. It was found that, as the temperature level of the inflowing gas streams increases, molecular collisions become more frequent and the gas mixing improves. Simulation results also led to the conclusion that an increase in temperature level of the heavier species produces more intense mixing, while, with an increase in inlet temperature of the lighter species, the parallel mixing diminishes.

In the present contribution, the alternative form of the proposed two-fluid model, which has been extended to more

realistic molecular interaction descriptions, is utilized for the analysis of the parallel mixing problem. Attention is focused here to clarify how mass disparity of the constituent may influence the degree of gas mixing. Moreover, the effect of molecular interaction descriptions in the prediction of the flow field is examined by comparing the results of the hard-sphere model, the Maxwell repulsive potential, and the Lennard-Jones 12-6 potential.

## 2. The two-fluid model

The alternative form of the two-fluid model leads to the following balance equations for the component species $\alpha$ [10]:

$$\frac{\partial}{\partial t}(n_\alpha m_\alpha) + \frac{\partial}{\partial \mathbf{x}} \cdot (n_\alpha m_\alpha \mathbf{v}_\alpha) = 0, \tag{1}$$

$$\frac{\partial}{\partial t}(n_\alpha m_\alpha \mathbf{v}_\alpha) + \frac{\partial}{\partial \mathbf{x}} \cdot (n_\alpha m_\alpha \mathbf{v}_\alpha \mathbf{v}_\alpha + \mathbf{P}_\alpha) = n_\alpha \mathbf{F}_\alpha + n_\alpha m_\alpha \upsilon_{\alpha\beta} \left(\tilde{\mathbf{v}}_\alpha - \mathbf{v}_\alpha\right), \tag{2}$$

$$\frac{\partial}{\partial t} E_\alpha + \frac{\partial}{\partial \mathbf{x}} . (E_\alpha \mathbf{v}_\alpha + \mathbf{q}_\alpha + \mathbf{P}_\alpha . \mathbf{v}_\alpha) = n_\alpha \mathbf{F}_\alpha . \mathbf{v}_\alpha + \upsilon_{\alpha\beta} \left(\tilde{E}_\alpha - E_\alpha\right), \tag{3}$$

as well as:

$$\frac{\partial}{\partial t}\left(n_\beta m_\beta\right) + \frac{\partial}{\partial \mathbf{x}} \cdot \left(n_\beta m_\beta \mathbf{v}_\beta\right) = 0, \tag{4}$$

$$\frac{\partial}{\partial t}\left(n_\beta m_\beta \mathbf{v}_\beta\right) + \frac{\partial}{\partial \mathbf{x}} \cdot \left(n_\beta m_\beta \mathbf{v}_\beta \mathbf{v}_\beta + \mathbf{P}_\beta\right) = n_\beta \mathbf{F}_\beta + n_\beta m_\beta \upsilon_{\beta\alpha} \left(\tilde{\mathbf{v}}_\beta - \mathbf{v}_\beta\right), \tag{5}$$

$$\frac{\partial}{\partial t} E_\beta + \frac{\partial}{\partial \mathbf{x}} \cdot \left(E_\beta \mathbf{v}_\beta + \mathbf{q}_\beta + \mathbf{P}_\beta . \mathbf{v}_\beta\right) = n_\beta \mathbf{F}_\beta . \mathbf{v}_\beta + \upsilon_{\beta\alpha} \left(\tilde{E}_\beta - E_\beta\right), \tag{6}$$

for the component species $\beta$. Here, $n_\alpha$ is the number density, $m_\alpha$ is the molecular mass, $\mathbf{v}_\alpha$ is the velocity vector, $\mathbf{q}_\alpha$ is the heat flux vector, $\mathbf{P}_\alpha$ is the pressure tensor, and $E_\alpha$ is the total energy per unit volume, all for constituent $\alpha$. Moreover, $\mathbf{F}_\alpha$ and $\mathbf{F}_\beta$ are the external force vectors. Meanwhile, $\upsilon_{\alpha\beta}$ and $\upsilon_{\beta\alpha}$ are the frequencies of cross-collision between $\alpha$ and $\beta$, which are calculated from;

$$\upsilon_{\alpha\beta} = \frac{16}{3} n_\beta \mathbf{\Omega}^{(1,1)}_{\alpha\beta}, \tag{7}$$

$$\upsilon_{\beta\alpha} = \frac{16}{3} n_\alpha \mathbf{\Omega}^{(1,1)}_{\beta\alpha}. \tag{8}$$

Here, $\mathbf{\Omega}^{(i,j)}_{\alpha\beta}$ and $\mathbf{\Omega}^{(i,j)}_{\beta\alpha}$ denote the Chapman–Cowling collision integrals [12] that depend on temperature and the law of interaction between particles. The values of these integrals for hard-sphere particles, Maxwellian particles, and for particles that interact according to a Lennard-Jones 12-6 potential are presented in Appendix A.

The collision parameters in Eqs. (2)–(6) are obtained from:

$$\tilde{\mathbf{v}}_\alpha = \tilde{\mathbf{v}}_\beta = \frac{m_\alpha \mathbf{v}_\alpha + m_\beta \mathbf{v}_\beta}{m_\alpha + m_\beta}, \tag{9}$$

$$\tilde{E}_\alpha = \rho_\alpha \left(\frac{R_\alpha \tilde{T}_\alpha}{\gamma_\alpha - 1} + \frac{\tilde{\mathbf{v}}^2_\alpha}{2}\right), \tag{10}$$

$$\tilde{E}_\beta = \rho_\beta \left(\frac{R_\beta \tilde{T}_\beta}{\gamma_\beta - 1} + \frac{\tilde{\mathbf{v}}^2_\beta}{2}\right), \tag{11}$$

$$\tilde{T}_\alpha = T_\alpha + 2\frac{m_\alpha m_\beta}{(m_\alpha + m_\beta)^2}\left((T_\beta - T_\alpha) + \frac{m_\beta}{6k}(\mathbf{v}_\alpha - \mathbf{v}_\beta)^2\right), \tag{12}$$

$$\tilde{T}_\beta = T_\beta + 2\frac{m_\alpha m_\beta}{(m_\alpha + m_\beta)^2}\left((T_\alpha - T_\beta) + \frac{m_\alpha}{6k}(\mathbf{v}_\beta - \mathbf{v}_\alpha)^2\right), \tag{13}$$

with $k$ being the Boltzmann constant and $R_\alpha = k/m_\alpha$ being the gas constant.

The evolution equations are supplemented by the constitutive relations for pressure tensor, as well as heat flux vector, which are:

$$P^\alpha_{ij} = n_\alpha k T_\alpha \delta_{ij} - \tau^\alpha_{ij}, \tag{14}$$

$$P^\beta_{ij} = n_\beta k T_\beta \delta_{ij} - \tau^\beta_{ij}, \tag{15}$$

$$q^\alpha_i = -\sum_{\gamma=1}^{2} \lambda_{\alpha\gamma} \frac{\partial T_\gamma}{\partial x_i} - M_{\alpha\alpha}(v^\alpha_i - v^\beta_i), \tag{16}$$

$$q^\beta_i = -\sum_{\gamma=1}^{2} \lambda_{\beta\gamma} \frac{\partial T_\gamma}{\partial x_i} - M_{\beta\alpha}(v^\alpha_i - v^\beta_i), \tag{17}$$

where:

$$\tau^\alpha_{ij} = 2\sum_{\gamma=1}^{2} \eta_{\alpha\gamma} \frac{\partial v^\gamma_{<i}}{\partial x_{j>}}, \tag{18}$$

$$\tau^\beta_{ij} = 2\sum_{\gamma=1}^{2} \eta_{\beta\gamma} \frac{\partial v^\gamma_{<i}}{\partial x_{j>}}, \tag{19}$$

with:

$$\frac{\partial v^\gamma_{<i}}{\partial x_{j>}} = \frac{1}{2}\left(\frac{\partial v^\gamma_i}{\partial x_j} + \frac{\partial v^\gamma_j}{\partial x_i}\right) - \frac{1}{3}\frac{\partial v^\gamma_k}{\partial x_k}\delta_{ij}. \tag{20}$$

These expressions represent a generalization of the laws of Navier–Stokes and Fourier. Here, $\eta_{\alpha\gamma}$, $\eta_{\beta\gamma}$, $\lambda_{\alpha\gamma}$, $\lambda_{\beta\gamma}$, $M_{\alpha\alpha}$ and $M_{\beta\alpha}$ are the transport coefficients associated with viscous, thermal, and thermal-diffusion effects. These coefficients are obtained from some kinetic relations that are presented in Appendix B.

## 3. Solution procedure

In the absence of external forces, the balance equations in a generalized curvilinear two-dimensional coordinate system become:

$$\frac{\partial \tilde{\mathbf{Q}}_\alpha}{\partial t} + \frac{\partial \tilde{\mathbf{F}}_\alpha}{\partial \xi} + \frac{\partial \tilde{\mathbf{G}}_\alpha}{\partial \eta} = \frac{\partial \tilde{\mathbf{F}}^\alpha_v}{\partial \xi} + \frac{\partial \tilde{\mathbf{G}}^\alpha_v}{\partial \eta} + \tilde{\mathbf{H}}_\alpha, \tag{21}$$

$$\frac{\partial \tilde{\mathbf{Q}}_\beta}{\partial t} + \frac{\partial \tilde{\mathbf{F}}_\beta}{\partial \xi} + \frac{\partial \tilde{\mathbf{G}}_\beta}{\partial \eta} = \frac{\partial \tilde{\mathbf{F}}^\beta_v}{\partial \xi} + \frac{\partial \tilde{\mathbf{G}}^\beta_v}{\partial \eta} + \tilde{\mathbf{H}}_\beta, \tag{22}$$

where:

$$\mathbf{Q}_\alpha = \begin{Bmatrix} E_\alpha \\ \rho_\alpha \\ \rho_\alpha u_\alpha \\ \rho_\alpha v_\alpha \end{Bmatrix}, \qquad \mathbf{F}_\alpha = \begin{Bmatrix} (E_\alpha + p_\alpha)u_\alpha \\ \rho_\alpha u_\alpha \\ \rho_\alpha u^2_\alpha + p_\alpha \\ \rho_\alpha u_\alpha v_\alpha \end{Bmatrix},$$

$$\mathbf{G}_\alpha = \begin{Bmatrix} (E_\alpha + p_\alpha)v_\alpha \\ \rho_\alpha v_\alpha \\ \rho_\alpha u_\alpha v_\alpha \\ \rho_\alpha v_\alpha^2 + p_\alpha \end{Bmatrix},$$

$$\mathbf{F}_v^\alpha = \begin{Bmatrix} u_\alpha \tau_{xx}^\alpha + v_\alpha \tau_{xy}^\alpha - q_x^\alpha \\ 0 \\ \tau_{xx}^\alpha \\ \tau_{xy}^\alpha \end{Bmatrix},$$

$$\mathbf{G}_v^\alpha = \begin{Bmatrix} u_\alpha \tau_{yx}^\alpha + v_\alpha \tau_{yy}^\alpha - q_y^\alpha \\ 0 \\ \tau_{yx}^\alpha \\ \tau_{yy}^\alpha \end{Bmatrix},$$

$$\mathbf{H}_\alpha = \begin{Bmatrix} \upsilon_{\alpha\beta}(\tilde{E}_\alpha - E_\alpha) \\ 0 \\ \rho_\alpha \upsilon_{\alpha\beta}(\tilde{u}_\alpha - u_\alpha) \\ \rho_\alpha \upsilon_{\alpha\beta}(\tilde{v}_\alpha - v_\alpha) \end{Bmatrix}, \tag{23}$$

$$\mathbf{Q}_\beta = \begin{Bmatrix} E_\beta \\ \rho_\beta \\ \rho_\beta u_\beta \\ \rho_\beta v_\beta \end{Bmatrix}, \qquad \mathbf{F}_\beta = \begin{Bmatrix} (E_\beta + p_\beta)u_\beta \\ \rho_\beta u_\beta \\ \rho_\beta u_\beta^2 + p_\beta \\ \rho_\beta u_\beta v_\beta \end{Bmatrix},$$

$$\mathbf{G}_\beta = \begin{Bmatrix} (E_\beta + p_\beta)v_\beta \\ \rho_\beta v_\beta \\ \rho_\beta u_\beta v_\beta \\ \rho_\beta v_\beta^2 + p_\beta \end{Bmatrix},$$

$$\mathbf{F}_v^\beta = \begin{Bmatrix} u_\beta \tau_{xx}^\beta + v_\beta \tau_{xy}^\beta - q_x^\beta \\ 0 \\ \tau_{xx}^\beta \\ \tau_{xy}^\beta \end{Bmatrix},$$

$$\mathbf{G}_v^\beta = \begin{Bmatrix} u_\beta \tau_{yx}^\beta + v_\beta \tau_{yy}^\beta - q_y^\beta \\ 0 \\ \tau_{yx}^\beta \\ \tau_{yy}^\beta \end{Bmatrix},$$

$$\mathbf{H}_\beta = \begin{Bmatrix} \upsilon_{\beta\alpha}(\tilde{E}_\beta - E_\beta) \\ 0 \\ \rho_\beta \upsilon_{\beta\alpha}(\tilde{u}_\beta - u_\beta) \\ \rho_\beta \upsilon_{\beta\alpha}(\tilde{v}_\beta - v_\beta) \end{Bmatrix}, \tag{24}$$

and:

$$\tilde{\mathbf{Q}}_\alpha = \frac{1}{J}\mathbf{Q}_\alpha, \qquad \tilde{\mathbf{F}}_\alpha = \frac{1}{J}(\mathbf{F}_\alpha \xi_x + \mathbf{G}_\alpha \xi_y),$$
$$\tilde{\mathbf{G}}_\alpha = \frac{1}{J}(\mathbf{F}_\alpha \eta_x + \mathbf{G}_\alpha \eta_y),$$
$$\tilde{\mathbf{F}}_v^\alpha = \frac{1}{J}(\mathbf{F}_v^\alpha \xi_x + \mathbf{G}_v^\alpha \xi_y),$$
$$\tilde{\mathbf{G}}_v^\alpha = \frac{1}{J}(\mathbf{F}_v^\alpha \eta_x + \mathbf{G}_v^\alpha \eta_y), \qquad \tilde{\mathbf{H}}_\alpha = \frac{1}{J}\mathbf{H}_\alpha, \tag{25}$$
$$\tilde{\mathbf{Q}}_\beta = \frac{1}{J}\mathbf{Q}_\beta, \qquad \tilde{\mathbf{F}}_\beta = \frac{1}{J}(\mathbf{F}_\beta \xi_x + \mathbf{G}_\beta \xi_y),$$
$$\tilde{\mathbf{G}}_\beta = \frac{1}{J}(\mathbf{F}_\beta \eta_x + \mathbf{G}_\beta \eta_y),$$
$$\tilde{\mathbf{F}}_v^\beta = \frac{1}{J}(\mathbf{F}_v^\beta \xi_x + \mathbf{G}_v^\beta \xi_y),$$
$$\tilde{\mathbf{G}}_v^\beta = \frac{1}{J}(\mathbf{F}_v^\beta \eta_x + \mathbf{G}_v^\beta \eta_y), \qquad \tilde{\mathbf{H}}_\beta = \frac{1}{J}\mathbf{H}_\beta, \tag{26}$$

with $J$ being the Jacobian of transformation.

Evidently, each set of balance equations bears a strong resemblance to the Navier–Stokes equations for a single-component flow. Consequently, the same numerical methods are applicable to these new equations. In this regard, a first-order explicit numerical procedure is utilized that leads to the following semi-discrete forms:

$$\begin{aligned} &\frac{\left(\hat{\mathbf{Q}}_{j,k}^\alpha\right)^{n+1} - \left(\hat{\mathbf{Q}}_{j,k}^\alpha\right)^n}{\Delta\tau} \\ &\quad + \left(\left(\hat{\mathbf{F}}_\alpha - \hat{\mathbf{F}}_v^\alpha\right)_{j+1/2,k} - (\hat{\mathbf{F}}_\alpha - \hat{\mathbf{F}}_v^\alpha)_{j-1/2,k}\right)^n \\ &\quad + \left(\left(\hat{\mathbf{G}}_\alpha - \hat{\mathbf{G}}_v^\alpha\right)_{j,k+1/2} - \left(\hat{\mathbf{G}}_\alpha - \hat{\mathbf{G}}_v^\alpha\right)_{j,k-1/2}\right)^n \\ &\quad = \left(\hat{\mathbf{H}}_{j,k}^\alpha\right)^n, \end{aligned} \tag{27}$$

and:

$$\begin{aligned} &\frac{\left(\hat{\mathbf{Q}}_{j,k}^\beta\right)^{n+1} - \left(\hat{\mathbf{Q}}_{j,k}^\beta\right)^n}{\Delta\tau} \\ &\quad + \left(\left(\hat{\mathbf{F}}_\beta - \hat{\mathbf{F}}_v^\beta\right)_{j+1/2,k} - \left(\hat{\mathbf{F}}_\beta - \hat{\mathbf{F}}_v^\beta\right)_{j-1/2,k}\right)^n \\ &\quad + \left(\left(\hat{\mathbf{G}}_\beta - \hat{\mathbf{G}}_v^\beta\right)_{j,k+1/2} - \left(\hat{\mathbf{G}}_\beta - \hat{\mathbf{G}}_v^\beta\right)_{j,k-1/2}\right)^n \\ &\quad = \left(\hat{\mathbf{H}}_{j,k}^\beta\right)^n, \end{aligned} \tag{28}$$

with $\Delta\xi = \Delta\eta = 1$. Here, $n$ is the time level and $\Delta\tau$ is the time-step. Moreover, the indices, $j$ and $k$, are attached to the $\xi$ and $\eta$ directions, respectively.

The equations can be expressed as:

$$\begin{aligned} \left(\hat{\mathbf{Q}}_{j,k}^\alpha\right)^{n+1} &= \left(\hat{\mathbf{Q}}_{j,k}^\alpha\right)^n \\ &\quad - \Delta\tau\left\{\left(\left(\hat{\mathbf{F}}_\alpha - \hat{\mathbf{F}}_\alpha^\nu\right)_{j+1/2,k} - \left(\hat{\mathbf{F}}_\alpha - \hat{\mathbf{F}}_\alpha^\nu\right)_{j-1/2,k}\right)^n\right. \\ &\quad + \left(\left(\hat{\mathbf{G}}_\alpha - \hat{\mathbf{G}}_\alpha^\nu\right)_{j,k+1/2} - \left(\hat{\mathbf{G}}_\alpha - \hat{\mathbf{G}}_\alpha^\nu\right)_{j,k-1/2}\right)^n \\ &\quad \left. - \left(\hat{\mathbf{H}}_{j,k}^\alpha\right)^n\right\}, \end{aligned} \tag{29}$$

and:

$$\begin{aligned} \left(\hat{\mathbf{Q}}_{j,k}^\beta\right)^{n+1} &= \left(\hat{\mathbf{Q}}_{j,k}^\beta\right)^n \\ &\quad - \Delta\tau\left\{\left(\left(\hat{\mathbf{F}}_\beta - \hat{\mathbf{F}}_\beta^\nu\right)_{j+1/2,k} - \left(\hat{\mathbf{F}}_\beta - \hat{\mathbf{F}}_\beta^\nu\right)_{j-1/2,k}\right)^n\right. \\ &\quad + \left(\left(\hat{\mathbf{G}}_\beta - \hat{\mathbf{G}}_\beta^\nu\right)_{j,k+1/2} - \left(\hat{\mathbf{G}}_\beta - \hat{\mathbf{G}}_\beta^\nu\right)_{j,k-1/2}\right)^n \\ &\quad \left. - \left(\hat{\mathbf{H}}_{j,k}^\beta\right)^n\right\}. \end{aligned} \tag{30}$$

Here, the viscous terms on the cell faces are calculated using a central differencing. Moreover, Roe's scheme [13] is applied to the inviscid terms. Solution of these two coupled systems of equations is straightforward since the procedure can be

repeated until summation of errors decreases to less than a desired value. The allowable time-step is calculated here based on the CFL (Courant–Friedrichs–Lewy) condition.

As the two sets of balance equations are solved for the constituents of the gas mixture, the mass density, velocity, and temperature of the whole mixture are obtained from the following kinetic relations:

$$\rho = \rho_\alpha + \rho_\beta, \tag{31}$$

$$\mathbf{v} = \frac{\rho_\alpha \mathbf{v}_\alpha + \rho_\beta \mathbf{v}_\beta}{\rho_\alpha + \rho_\beta}, \tag{32}$$

$$T = \frac{n_\alpha T_\alpha + n_\beta T_\beta}{n_\alpha + n_\beta}. \tag{33}$$

## 4. Simulation results

Initially, a code validation study is undertaken. For this purpose, a mixture flow of He–Xe between two parallel plates is simulated. The lengths of the plates are 0.01 m, and the plates are 0.001 m apart. They are also considered adiabatic. The inlet stagnation pressure and temperature are 10 kPa and 300 K, respectively, and the inlet concentration ($\rho_{He}/\rho_{He} + \rho_{Xe}$) is 0.5. Moreover, the outlet pressure is 7.5 kPa. Since the Knudsen numbers of the constituents, as well as the overall Knudsen number of the whole mixture, remain below 0.001 over the entire flow field, the no-slip condition is still valid at the plates. It is noteworthy that the overall Knudsen number of a gas mixture is defined as $Kn_{overall} = \lambda_{overall}/L$, with $\lambda_{overall}$ being the overall mean-free-path of the mixture and $L$ being the characteristic length of the problem. Recent kinetic analysis of Zahmatkesh et al. [14] has demonstrated that the overall mean-free-path in a binary system takes the form of $\lambda_{overall} = (\rho_\alpha\lambda_\alpha + \rho_\beta\lambda_\beta)/(\rho_\alpha + \rho_\beta)$, with $\lambda_\alpha$ and $\lambda_\beta$ being the mean-free-paths of the constituents.

The problem is solved employing 1891 ($61 \times 31$) nodes based on a grid refinement study. In what concerns the midplane distributions of pressure, temperature and Mach number, the results of the current two-fluid model with the hard-sphere molecular interaction description are compared with those of the Navier–Stokes equations in Figures 1–3. Clearly, the two approaches lead to almost the same simulation results. The small discrepancies are not surprising since the methods for the use of transport coefficients are completely distinct in these two approaches. Indeed, during the Navier–Stokes computation, the viscosity and thermal conductivity of the constituents are input externally. Thereafter, properties of the mixture as a whole are estimated in terms of these parameters from some semi-empirical correlations. This may produce some errors in the corresponding results. In contrast, the current two-fluid model calculates transport coefficients from some kinetic relations, which makes it more accurate.

The appearance of the excellent agreement between the results of the two-fluid model and those of the Navier–Stokes equations provides confidence in the developed mathematical model, as well as the employed solution procedure, for further studies. Consequently, in what follows, the same methodology is used to analyze the gas mixing problem.

A schematic of the mixing flow system is depicted in Figure 4. Here, parallel streams of two gases, which are initially separated by a splitter plate, enter the mixing chamber. The computations are undertaken for two-fluid systems, namely, He–Xe and Ne–Ar. The molar masses of the constituents are $M_{He} = 4.0026$, $M_{Ne} = 20.183$, $M_{Ar} = 39.948$ and $M_{Xe} = 131.30$ in atomic units. Consequently, the study includes one mixture with particles of about equal mass and another one with particles of quite distinct mass. This will clarify how the mass disparity of the constituents may affect the establishment of the flow field. In both of the mixture problems, the lighter species is regarded as the inflowing upper stream. The flow properties of these two-fluid systems are maintained identical, which are:

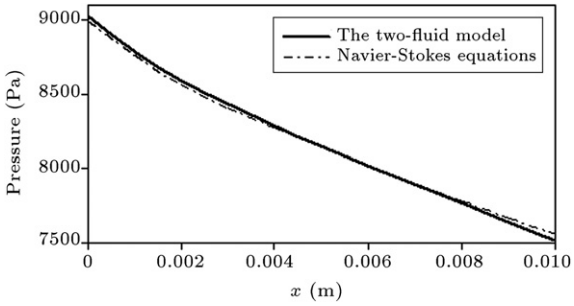


Figure 1: Midplane distribution of pressure.

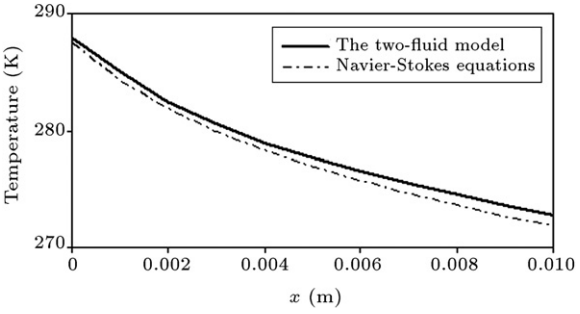


Figure 2: Midplane distribution of temperature.

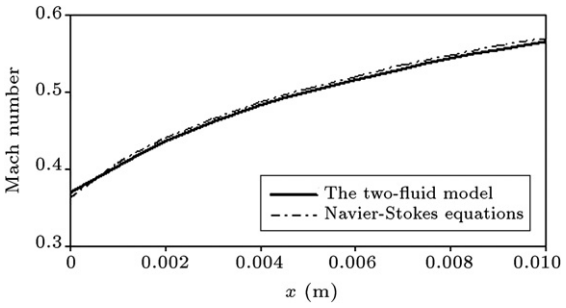


Figure 3: Midplane distribution of Mach number.

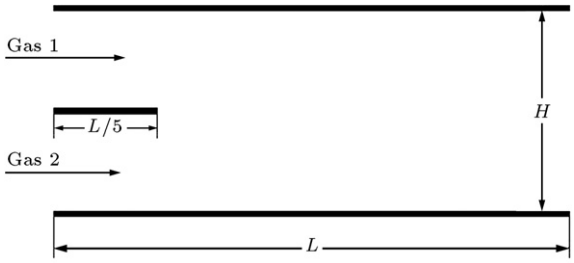


Figure 4: The mixing flow system.

*Problem geometry*

Length of plates : $L = 0.1$ m,

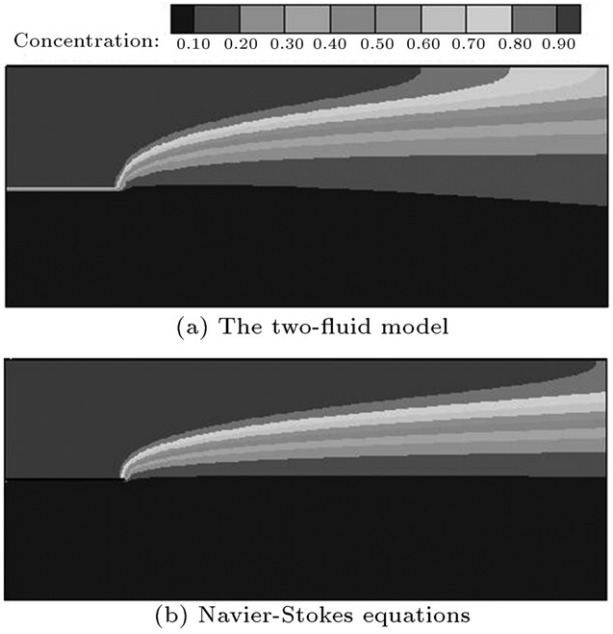


Figure 5: Mixing pattern for the He–Xe flow system.

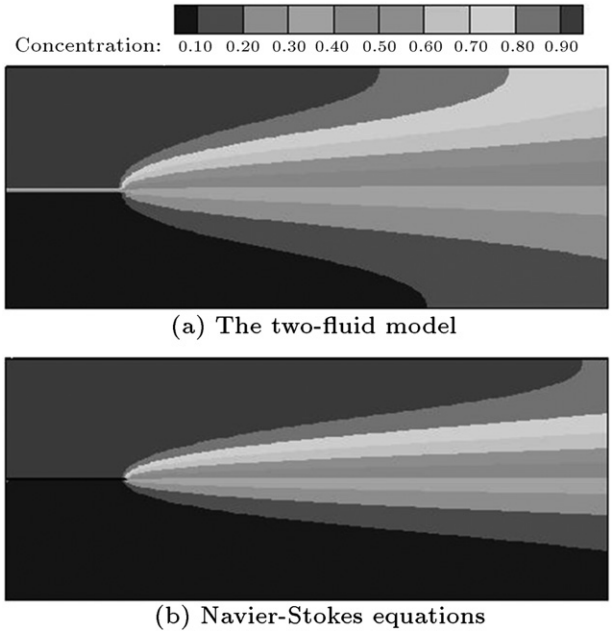


Figure 6: Mixing pattern for the Ne–Ar flow system.

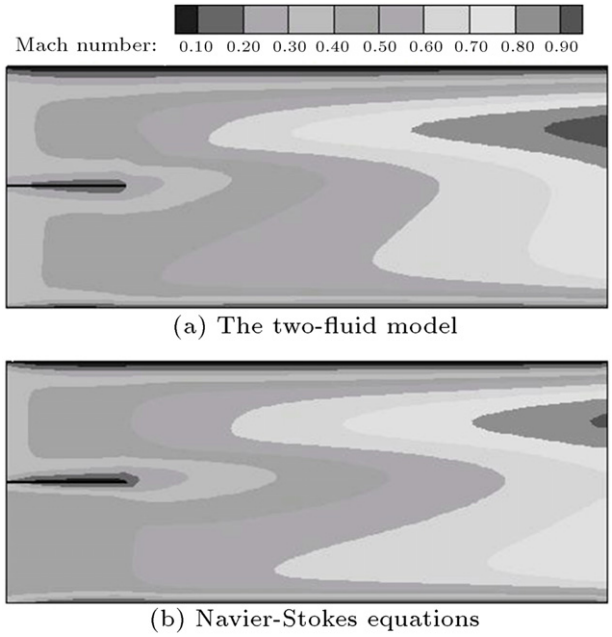


Figure 7: Mach number contours for the He–Xe flow system.

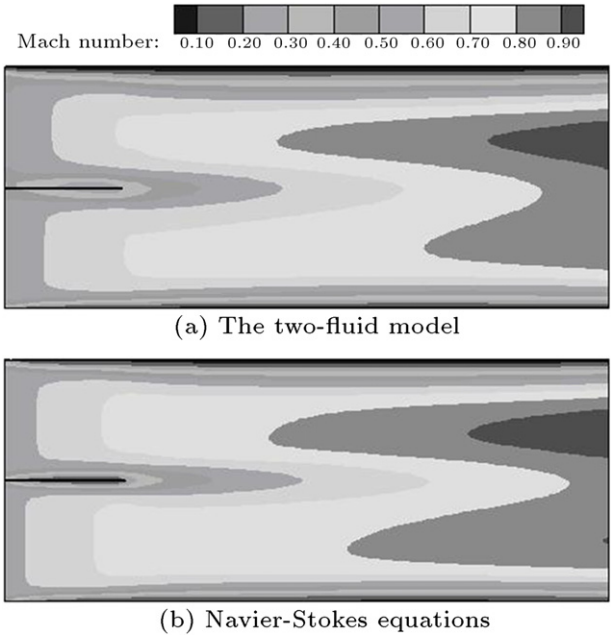


Figure 8: Mach number contours for the Ne–Ar flow system.

Distance between plates : $H = 0.01$ m.

*Inlet conditions*

Stagnation pressure : $p_{t,i} = 15$ kPa,

Stagnation temperature : $T_{t,i} = 300$ K.

*Exit condition*

Pressure : $p_e = 7.5$ kPa.

Moreover, the splitter plate and the walls of the mixing chamber are considered adiabatic.

Under this circumstance, the Knudsen numbers of the constituents, as well as the overall Knudsen number of the whole mixture, remain below 0.001 over the entire flow field. Consequently, the no-slip condition is still applicable to the walls as well as the splitter plate.

The problems are solved using 7171 ($101 \times 71$) nodes based on a grid refinement study. Results, in terms of the mixing pattern of the two gas streams, are compared with those of the Navier–Stokes equations in Figures 5 and 6. The presented results correspond to the hard-sphere molecular interaction model. Here and henceforth, the cross-streamwise direction is stretched by a factor of 4 for better depiction. Comparing the simulation results of the two-fluid systems indicates that while Xe gas rapidly diffuses towards the He flow, mixing is intense

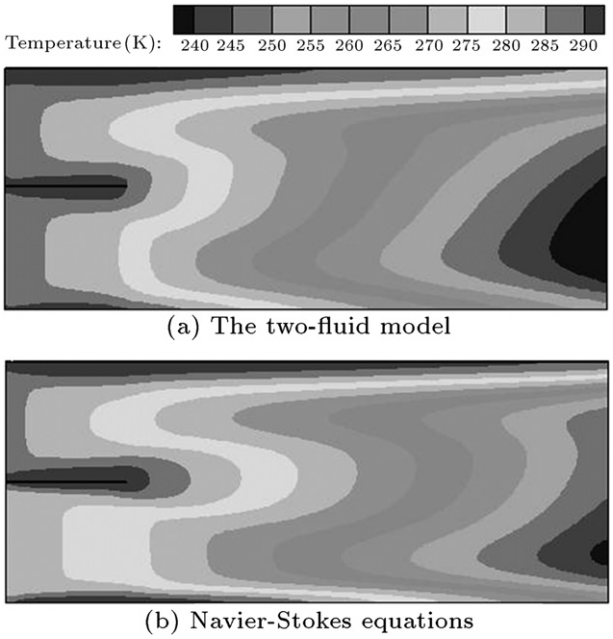


Figure 9: Temperature contours for the He–Xe flow system.

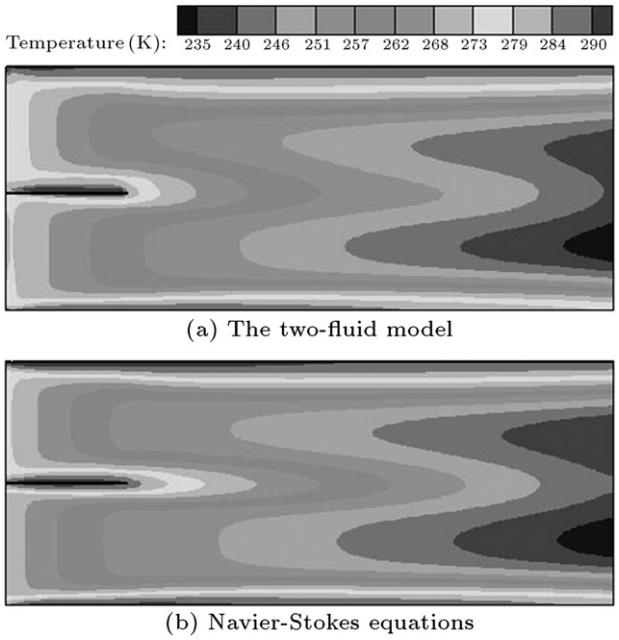


Figure 10: Temperature contours for the Ne–Ar flow system.

in the Ne–Ar system. Concerning this, one may conclude that as differences in the molecular mass of the two gas streams decreases, the parallel mixing becomes more effective. Closer scrutiny of Figures 5 and 6 reveals that the two-fluid model is more diffusive since it predicts faster mixing. This is in accord with previous observations of Zahmatkesh et al. [9] in some nozzle flow problems. Here, the results of the two-fluid model may be more accurate since they automatically describe diffusion processes excluding the use of any coefficients for ordinary, pressure, and thermal diffusion, which are generally required during Navier–Stokes computation of gas mixture flows.

The discrepancies that appear in the diffusion pattern of the aforesaid approaches produce some differences in their simulation results. This is obvious in Figures 7–10, where contour plots of Mach number and temperature are provided. Inspection of the figures indicates that for the Ne–Ar system, the distributions of Mach number and temperature are more symmetric about the splitter plate. The figures also demonstrate that the Ne–Ar system provides higher flow acceleration. This occurs since the corresponding cross-streamwise velocities are much lower there. Such behavior allows one to conclude that as the difference in the molecular mass of the two gas streams decreases, the flow acceleration enhances, and the distributions of Mach number and temperature become more symmetric about the splitter plate. Closer scrutiny of Figures 7–10 reveals that the predictions of the two-fluid model and the Navier–Stokes equations for temperature and Mach number are almost identical for the Ne–Ar system, but different for the He–Xe system. Physical reasoning for such behavior is the fact that the exchange of energy through molecular collisions takes a longer time interval for disparate mass gas mixtures than for similar mass gas mixtures. This indicates that when the molecular masses of the two gas streams are quite distinct, the two-fluid model is preferable to the Navier–Stokes equations.

Finally, the effect of molecular interaction descriptions on the prediction of the flow field is analyzed. For this purpose, the results of the hard-sphere model, the Maxwell repulsive potential and the Lennard-Jones 12-6 potential, in

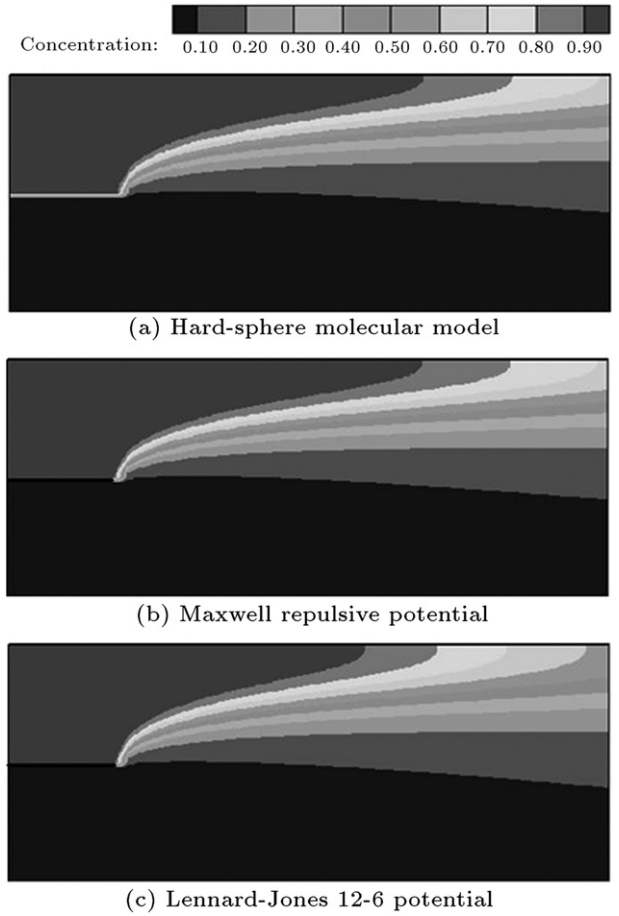


Figure 11: Effect of molecular interaction description on the two-fluid prediction of mixing pattern for the He–Xe flow system.

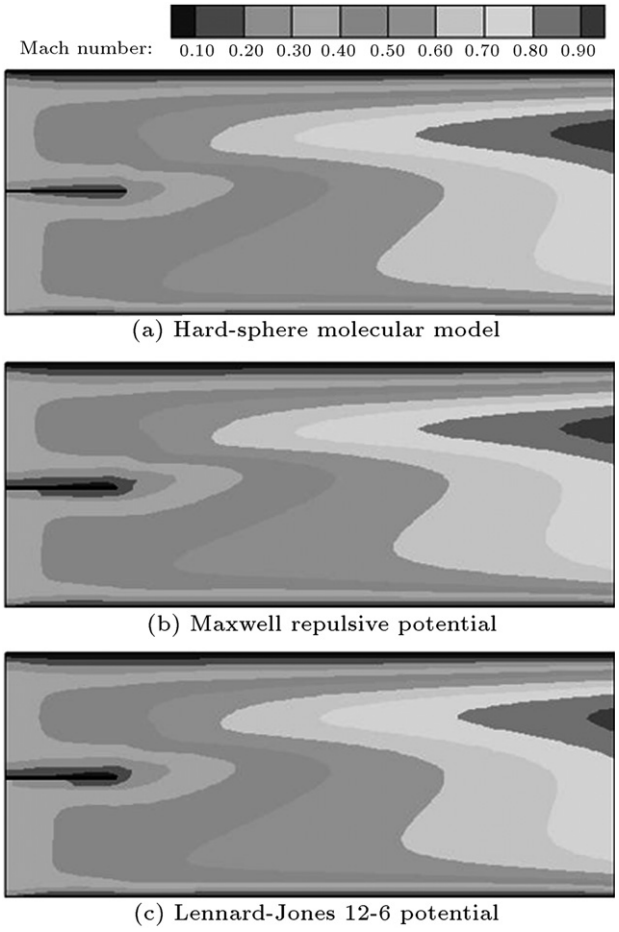


Figure 12: Effect of molecular interaction description on the two-fluid prediction of Mach number for the He–Xe flow system.

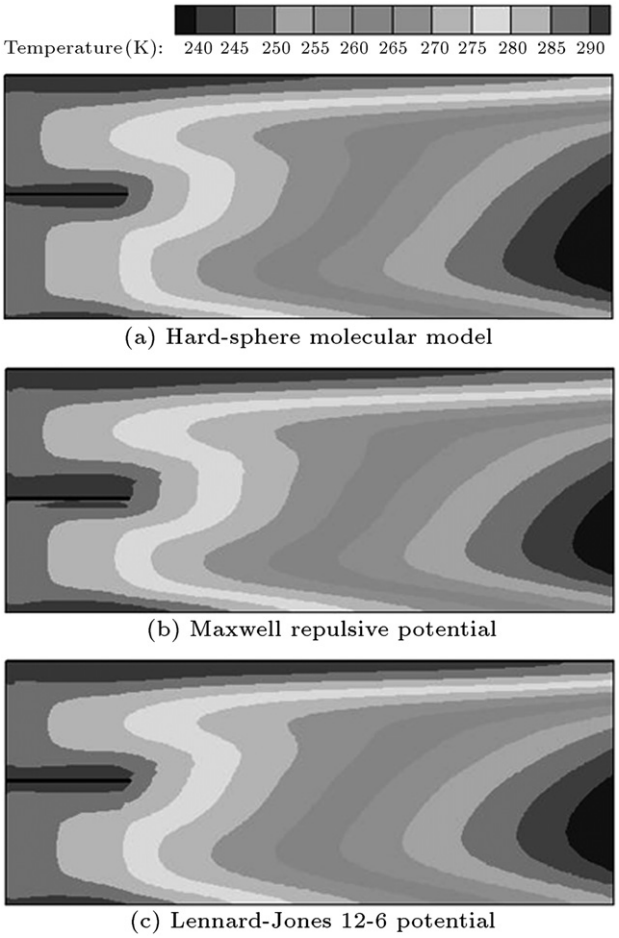


Figure 13: Effect of molecular interaction description on the two-fluid prediction of temperature for the He–Xe flow system.

terms of mixing pattern, as well as the distributions of Mach number and temperature, are compared in Figures 11–13 which corresponds to the He–Xe flow system. Inspection of the figures provides evidence that the choice of molecular interaction model does not make a substantial difference in the simulation results. Nevertheless, it is obvious that the Lennard-Jones 12-6 potential is the most diffusive molecular model. This is in accordance with previous observations of Zahmatkesh et al. [10] in nozzle flow fields.

## 5. Concluding remarks

A recently proposed two-fluid model was successfully employed here to simulate the mixing pattern of two parallel gas streams, initially separated by a splitter plate. Inspection of the presented results indicated that when the molecular masses of the two gas streams are quite distinct, the two-fluid model is preferable to the Navier–Stokes equations. Moreover, it was found that as differences in the molecular masses of the two gas streams decrease: (i) the flow acceleration enhances, (ii) the distributions of Mach number and temperature become more symmetric about the splitter plate, and (iii) the parallel mixing becomes more effective. Although the choice of molecular interaction model did not make a substantial difference to the simulation results, it was found that the Lennard-Jones 12-6 potential is the most diffusive molecular model.

## Acknowledgment

Iman Zahmatkesh, the first author, is grateful to Prof. Marques Jr. for sending him a copy of his Ph.D. Thesis and for many inspiring discussions.

## Appendix A

The values of the Chapman–Cowling collision integrals for the employed molecular interaction models are as follows:

### A.1. Hard-sphere model

In this model, the particles are pictured as rigid impenetrable spheres with an interparticle potential function in the form of:

$$\phi_{\alpha\beta}(r) = \begin{cases} \infty & r < (d_\alpha + d_\beta)/2 \\ 0 & r > (d_\alpha + d_\beta)/2 \end{cases} \quad \text{(A.1)}$$

Here, $d_\alpha$ and $d_\beta$ are the molecular diameters and $r$ is the intermolecular separation. As can be observed, it works on the simple premise that interaction occurs only when molecules come into actual physical contact.

Here, the Chapman–Cowling collision integrals can be computed exactly, which take the following form [12]:

$$\Omega_{\alpha\beta}^{(i,j)} = \left(\frac{d_\alpha + d_\beta}{4}\right)^2 \left(\frac{2\pi kT}{m_{\alpha\beta}}\right)^{\frac{1}{2}} \times \left[1 - \frac{1+(-1)^i}{2(i+1)}\right](j+1)!, \tag{A.2}$$

with $m_{\alpha\beta} = m_\alpha m_\beta/(m_\alpha + m_\beta)$ being the reduced mass.

### A.2. Maxwell repulsive potential

In this molecular interaction description, the interparticle potential function is approximated by:

$$\phi_{\alpha\beta}(r) = \frac{\kappa_{\alpha\beta}}{4}\frac{1}{r^4}, \tag{A.3}$$

with $\kappa_{\alpha\beta}$ being a constant of proportionality in the force law. This potential is also purely repulsive, but corrects the exaggerated steepness of the hard-sphere model.

Here, the Chapman–Cowling collision integrals are expressed as [12]:

$$\Omega_{\alpha\beta}^{(i,j)} = \frac{1}{2}\left(\frac{2\pi kT}{m_{\alpha\beta}}\right)^{\frac{1}{2}} \left(\frac{\kappa_{\alpha\beta}}{2kT}\right)^{\frac{1}{2}} A_i(5)\Gamma\left(j+\frac{3}{2}\right), \tag{A.4}$$

with $A_i(5)$ being tabulated pure numbers and $\Gamma$ being the gamma function.

### A.3. Lennard-Jones 12-6 potential

In actual gases, intermolecular forces are repulsive at small distances and weakly attractive at large distances. Such behavior is most simply described by the Lennard-Jones 12-6 potential in the form of:

$$\phi_{\alpha\beta}(r) = 4\varepsilon_{\alpha\beta}\left[\left(\frac{\sigma_{\alpha\beta}}{r}\right)^{12} - \left(\frac{\sigma_{\alpha\beta}}{r}\right)^{6}\right], \tag{A.5}$$

where $\varepsilon_{\alpha\beta}$ is the maximum energy of attraction, $\sigma_{\alpha\beta}$ is the distance at which the potential function of interaction vanishes, and $r$ is the intermolecular separation.

Here, the Chapman–Cowling collision integrals become [12]:

$$\Omega_{\alpha\beta}^{(i,j)} = \sigma_{\alpha\beta}^2 \left(\frac{2\pi kT}{m_{\alpha\beta}}\right)^{\frac{1}{2}} W_{\alpha\beta}^{(i,j)}. \tag{A.6}$$

The values of the non-dimensional integrals, $W_{\alpha\beta}^{(i,j)}$, depend on the reduced temperature, $kT/\varepsilon_{\alpha\beta}$, and can be found elsewhere [15].

## Appendix B

In the current two-fluid model, the transport coefficients that appear in the constitutive relations are calculated from the following kinetic relations [16]:

$$\eta_{\alpha\alpha} = \frac{x_\alpha kTA_4}{A_1A_4 - A_2A_3}, \qquad \eta_{\alpha\beta} = \frac{x_\beta kTA_2}{A_1A_4 - A_2A_3}, \tag{B.1}$$

$$\eta_{\beta\alpha} = \frac{x_\alpha kTA_3}{A_1A_4 - A_2A_3}, \qquad \eta_{\beta\beta} = \frac{x_\beta kTA_1}{A_1A_4 - A_2A_3}, \tag{B.2}$$

$$\lambda_{\alpha\alpha} = \frac{5k}{2m_\alpha}\frac{x_\alpha kTB_4}{B_1B_4 - B_2B_3}, \tag{B.3}$$

$$\lambda_{\alpha\beta} = \frac{5k}{2m_\beta}\frac{x_\beta kTB_2}{B_1B_4 - B_2B_3},$$

$$\lambda_{\beta\alpha} = \frac{5k}{2m_\alpha}\frac{x_\alpha kTB_3}{B_1B_4 - B_2B_3},$$

$$\lambda_{\beta\beta} = \frac{5k}{2m_\beta}\frac{x_\beta kTB_1}{B_1B_4 - B_2B_3}, \tag{B.4}$$

$$M_{\alpha\alpha} = \frac{p_\alpha x_\beta C(z_\alpha^2 B_2 - z_\beta^2 B_4)}{B_1B_4 - B_2B_3},$$

$$M_{\beta\alpha} = \frac{p_\beta x_\alpha C(z_\alpha^2 B_1 - z_\beta^2 B_3)}{B_1B_4 - B_2B_3}. \tag{B.5}$$

where:

$$A_1 = \frac{8}{5}x_\alpha\Omega_{\alpha\alpha}^{(2,2)} + \frac{16}{5}x_\beta z_\beta\Omega_{\alpha\beta}^{(1,1)}\left(\frac{10}{3}z_\alpha + z_\beta\frac{\Omega_{\alpha\beta}^{(2,2)}}{\Omega_{\alpha\beta}^{(1,1)}}\right), \tag{B.6}$$

$$A_2 = \frac{16}{5}x_\alpha z_\alpha z_\beta\Omega_{\alpha\beta}^{(1,1)}\left(\frac{10}{3} - \frac{\Omega_{\alpha\beta}^{(2,2)}}{\Omega_{\alpha\beta}^{(1,1)}}\right), \tag{B.7}$$

$$A_3 = \frac{16}{5}x_\beta z_\alpha z_\beta\Omega_{\alpha\beta}^{(1,1)}\left(\frac{10}{3} - \frac{\Omega_{\alpha\beta}^{(2,2)}}{\Omega_{\alpha\beta}^{(1,1)}}\right), \tag{B.8}$$

$$A_4 = \frac{8}{5}x_\beta\Omega_{\beta\beta}^{(2,2)} + \frac{16}{5}x_\alpha z_\alpha\Omega_{\alpha\beta}^{(1,1)}\left(\frac{10}{3}z_\beta + z_\alpha\frac{\Omega_{\alpha\beta}^{(2,2)}}{\Omega_{\alpha\beta}^{(1,1)}}\right), \tag{B.9}$$

$$B_1 = \frac{16}{15}x_\alpha\Omega_{\alpha\alpha}^{(2,2)} + \frac{16}{3}x_\beta z_\beta\Omega_{\alpha\beta}^{(1,1)}\left[3z_\alpha^2 + z_\beta^2\left(\frac{5}{2} - 2\frac{\Omega_{\alpha\beta}^{(1,2)}}{\Omega_{\alpha\beta}^{(1,1)}} + \frac{2}{5}\frac{\Omega_{\alpha\beta}^{(1,3)}}{\Omega_{\alpha\beta}^{(1,1)}}\right) + \frac{4}{5}z_\alpha z_\beta\frac{\Omega_{\alpha\beta}^{(2,2)}}{\Omega_{\alpha\beta}^{(1,1)}}\right], \tag{B.10}$$

$$B_2 = \frac{16}{3}x_\alpha z_\alpha z_\beta^2\Omega_{\alpha\beta}^{(1,1)}\left[\frac{11}{2} - 2\frac{\Omega_{\alpha\beta}^{(1,2)}}{\Omega_{\alpha\beta}^{(1,1)}} + \frac{2}{5}\frac{\Omega_{\alpha\beta}^{(1,3)}}{\Omega_{\alpha\beta}^{(1,1)}} - \frac{4}{5}\frac{\Omega_{\alpha\beta}^{(2,2)}}{\Omega_{\alpha\beta}^{(1,1)}}\right], \tag{B.11}$$

$$B_3 = \frac{16}{3}x_\beta z_\beta z_\alpha^2\Omega_{\alpha\beta}^{(1,1)}\left[\frac{11}{2} - 2\frac{\Omega_{\alpha\beta}^{(1,2)}}{\Omega_{\alpha\beta}^{(1,1)}} + \frac{2}{5}\frac{\Omega_{\alpha\beta}^{(1,3)}}{\Omega_{\alpha\beta}^{(1,1)}} - \frac{4}{5}\frac{\Omega_{\alpha\beta}^{(2,2)}}{\Omega_{\alpha\beta}^{(1,1)}}\right], \tag{B.12}$$

$$B_4 = \frac{16}{15}x_\beta\Omega_{\beta\beta}^{(2,2)} + \frac{16}{3}x_\alpha z_\alpha\Omega_{\alpha\beta}^{(1,1)}\left[3z_\beta^2 + z_\alpha^2\left(\frac{5}{2} - 2\frac{\Omega_{\alpha\beta}^{(1,2)}}{\Omega_{\alpha\beta}^{(1,1)}} + \frac{2}{5}\frac{\Omega_{\alpha\beta}^{(1,3)}}{\Omega_{\alpha\beta}^{(1,1)}}\right) + \frac{4}{5}z_\alpha z_\beta\frac{\Omega_{\alpha\beta}^{(2,2)}}{\Omega_{\alpha\beta}^{(1,1)}}\right], \tag{B.13}$$

$$C = \frac{40}{3}\Omega_{\alpha\beta}^{(1,1)}\left(1 - \frac{2}{5}\frac{\Omega_{\alpha\beta}^{(1,2)}}{\Omega_{\alpha\beta}^{(1,1)}}\right), \tag{B.14}$$

with $x_i = n_i/(n_\alpha + n_\beta)$ and $z_i = m_i/(m_\alpha + m_\beta)$. These expressions clarify how the choice of molecular interaction model may influence the transport properties through the Chapman–Cowling collision integrals.

## References


[1] Kamali, R., Emdad, H. and Alishahi, M.M. "The importance of thermal mass diffusion effects in solution of Navier–Stokes equations for some gas mixture problems", *Fluid Dyn. Res.*, 37, pp. 173–182 (2005).

[2] Goldman, E. and Sirovich, L. "Equations for gas mixtures", *Phys. Fluids*, 10, pp. 1928–1940 (1967).

[3] Elizarova, T.G., Graur, I.A. and Lengrand, J.C. "Two-fluid computational model for a binary gas mixture", *Eur. J. Mech. B Fluids*, 20, pp. 351–369 (2001).

[4] Tahiri, E.E., Tij, M. and Garzo, V. "Nonlinear transport in a binary mixture in the presence of gravitation", *Physica A*, 297, pp. 97–114 (2001).

[5] Fernandes, A.S. and Marques Jr., W. "Sound propagation in binary gas mixtures from a kinetic model of the Boltzmann equation", *Physica A*, 332, pp. 29–46 (2004).

[6] Kosuge, S. "Model Boltzmann equation for gas mixtures: construction and numerical comparison", *Eur. J. Mech. B Fluids*, 28, pp. 170–184 (2009).

[7] Kamali, R., Emdad, H. and Alishahi, M.M. "A new set of conservation equations based on the kinetic theory applied to gas mixture problems", *Scientia Iranica*, 14, pp. 458–466 (2007).

[8] Kamali, R., Emdad, H. and Alishahi, M.M. "Multicomponent fluid flow analysis using a new set of conservation equations", *Fluid Dyn. Res.*, 40, pp. 343–363 (2008).

[9] Zahmatkesh, I., Emdad, H. and Alishahi, M.M. "Viscous and inviscid solutions of some gas mixture problems", *Heat Transfer Res.*, 42, pp. 233–250 (2011).

[10] Zahmatkesh, I., Emdad, H. and Alishahi, M.M. "Importance of molecular interaction description on the hydrodynamics of gas mixtures", *Scientia Iranica, Trans. B: Mech. Eng.*, 18, pp. 1287–1296 (2011).

[11] Zahmatkesh, I., Emdad, H. and Alishahi, M.M. "Effect of temperature level on parallel mixing of two gas streams", *Mech. Res. Commun.*, 38, pp. 141–145 (2011).

[12] Chapman, S. and Cowling, T.G., *The Mathematical Theory of Non-Uniform Gases*, Cambridge University Press, Cambridge (1970).

[13] Roe, P.L. "Discrete models for numerical analysis of time-dependent multidimensional gas dynamics", *J. Comput. Phys.*, 63, pp. 458–476 (1986).

[14] Zahmatkesh, I., Alishahi, M.M. and Emdad, H. "New velocity-slip and temperature-jump boundary conditions for Navier–Stokes computation of gas mixture flows in microgeometries", *Mech. Res. Commun.*, 38, pp. 417–424 (2011).

[15] Hirschfelder, J.Q., Bird, R.B. and Spotz, E.L. "The transport properties for non-polar gases", *J. Chem. Phys.*, 16, pp. 968–981 (1948).

[16] Marques, W. Jr. "Calculation of scattering spectra in mixtures of monatomic ideal gases: A contribution to the extended thermodynamics (Berechnung von streuspektren in mischungen einatomiger idealer gase: ein beitrag zur erweiterten thermodynamik)", Ph.D. Thesis, TU-Berlin (1994).



**Iman Zahmatkesh** is Assistant Professor of Mechanical Engineering at Islamic Azad University, Mashhad Branch. He earned his B.S. and M.S. degrees in Mechanical Engineering from Ferdowsi University of Mashhad, Iran, and a Ph.D. degree in the same subject from Shiraz University, Iran. He has published more than ten ISI papers in distinct areas of computational fluid dynamics.

**Homayoun Emdad** is Associate Professor of Mechanical Engineering at Shiraz University, Iran. He earned his B.S. degree in Aerospace Engineering from Washington University, USA, and M.S. and Ph.D. degrees in the same subject from Kansas University, USA. His research interests are computational fluid dynamics, aerodynamics, fluid mechanics and two phase flow analysis.

**Mohammad Mehdi Alishahi** is Professor of Mechanical Engineering at Shiraz University, Iran. He earned his B.S. degree in Aerospace Engineering from Sharif University of Technology, Tehran, Iran, and M.S. and Ph.D. degrees in the same subject from Massachusetts Institute of Technology, USA. His main research interests are computational fluid dynamics, aerodynamics, and fluid mechanics.